THE JOURNAL OF PHYSICAL CHEMISTRY B

Article

pubs.acs.org/JPCB

Molecular Insights into the D1R Agonist and D2R/D3R Antagonist Effects of the Natural Product (−)-Stepholidine: Molecular Modeling and Dynamics Simulations

Bian Li,[†,§] Wei Li,[†,§] Peng Du,[†,§] Kun Qian Yu,*[,‡] and Wei Fu*[,†]

[†]Department of Medicinal Chemistry & Key Laboratory of Smart Drug Delivery, Ministry of Education & PLA, School of Pharmacy, Fudan University, Shanghai 201203, China

[‡]Drug Discovery and Design Center, State Key Laboratory of Drug Research, Shanghai Institute of Materia Medica, Chinese Academy of Sciences, Shanghai 201203, China

Supporting Information

ABSTRACT: (−)-Stepholidine (*l*-SPD), an active ingredient of the Chinese herb *Stephania*, is the first compound found to have a dual function as a dopamine receptor D1 agonist and D2 antagonist. The preliminary dynamical behaviors of D1R and D2R and their interaction modes with *l*-SPD were investigated in our previous study. Recently, the pharmacological effect of *l*-SPD on D3R was elucidated as an antagonist. This new discovery in combination with the explosion of structural biology in GPCR superfamily prompted us to perform a more comprehensive investigation on the special pharmacological profiles of *l*-SPD on dopamine receptors. In this study, the integration of homology modeling, automated molecular docking, and MD simulations was used to probe the agonistic and antagonistic mechanism of *l*-SPD on D1R, D2R, and D3R. Our analyses showed that hydrogen bonding of the hydroxyl group on the D ring of *l*-SPD with side chain of N6.55 which, in combination with hydrophobic stacking between I3.40, F6.44 and W6.48, is the key feature to mediate the agonist effect of *l*-SPD on D1R, whereas the absence of hydrophobic stacking between I3.40, F6.44, and W6.48 in D2R and D3R excludes receptor activation. Finally, the agonistic and antagonistic mechanisms of *l*-SPD and an activation model of D1R were proposed on the basis of these findings. The present study could guide future experimental works on these receptors and has the significance to the design of functionally selective drugs targeting dopamine receptors.

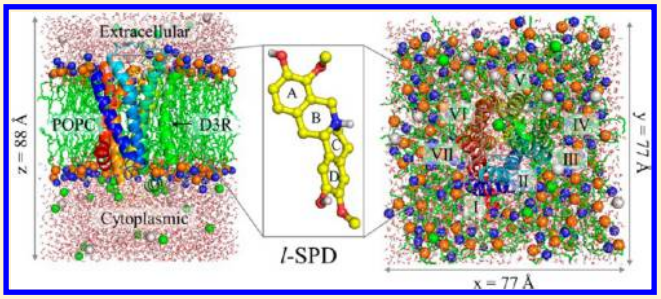

INTRODUCTION

G-protein-coupled receptors (GPCRs) are the largest family of integral membrane proteins that mediate most of physiological responses to hormones, neurotransmitters, and environmental stimulants. GPCRs constitute the largest class of therapeutic targets as evidenced by the fact that at least one-fourth of drugs on the market exert their therapeutic activity by modulating rhodopsin-like GPCRs.[1] In the past 3 years, there were remarkable advances in the crystallography of G-protein-coupled receptors (GPCRs). Highlights have included the characterization of the crystal structures of antagonist-bound and agonist-bound GPCRs: the human β_2 adrenergic receptor (β_2AR),[2−5] the turkey β_1AR,[6,7] the human A_{2A} adenosine receptor,[8,9] the human chemokine receptor CXCR4,[10] and the human dopamine D3 receptor.[11] The availability of such high-resolution crystal structures can greatly help to guide the structure-based GPCR drug discovery. However, with the inactive-state structures of β_2AR, β_1AR, and A_{2A} receptor, medicinal chemists could probably only be able to develop ligands that stabilize the inactive conformation. The agonistic mechanism of GPCRs based on homology modeling taking these inactive-state receptors as template is also problematic. The newly available active-state structures of β_2AR, β_1AR, and A_{2A} receptor thus provide a solid basis for the elucidation of the conformational changes associated with agonist binding.

Dopamine (DA), the endogenous ligand of dopaminergic neurotransmission systems, has been associated with many physiological functions such as fine movement coordination, cognition, and emotion. DA exerts its effects by activating five distinct dopamine receptors (DRs) which belong to the GPCR superfamily and are classified into two subfamilies: D1-like (D1R and D5R) and D2-like (D2R, D3R, and D4R) based on their pharmacological and functional characteristics. It has been established that DRs are primary targets of antipsychotic drugs used to treat psychomotor diseases such as schizophrenia, a debilitating mental illness which affects 0.5−1.5% of the worldwide population.[12] The pathogenesis of schizophrenia is suggested to be related to dysfunction of the D1R in the medial

Received: May 21, 2012
Revised: June 14, 2012
Published: June 15, 2012

prefrontal cortex (mPFC), which is accompanied by D2R hyperactivity in subcortical regions such as the ventral tegmental area (VTA) and the nucleus accumbens (NAc). The D1R dysfunction is believed to be responsible for the negative symptoms of schizophrenia, whereas the D2R hyperactivity might lead to the positive symptoms of the disorder.[13−15] Thus, an effective antipsychotic drug should simultaneously possess D1R agonistic and D2R antagonistic activities.[15]

(−)-Stepholidine (*l*-SPD), an active natural compound isolated from the Chinese herb *Stephania*, is to date the only drug with a dual effect as a D1R agonist and D2R antagonist. *l*-SPD displays high affinity to D1- and D2-like receptors but low affinity to 5-HT_2 receptors and rare affinity to several other neurotransmitter receptors.[15−17] Moreover, clinical investigations showed that *l*-SPD is superior to perphenazine in antipsychotic efficacy.[18] Unlike perphenazine, *l*-SPD does not induce any extrapyramidal symptoms (EPS),[19] making it an attractive compound in studying the dual action mechanism of a chemical for developing novel antipsychotics.[18] The recent discovery that *l*-SPD has an antagonistic effect on D3R rendered both *l*-SPD and D3R much more intriguing. However, the complete molecular basis of the dual action mechanism of *l*-SPD still remains obscure despite it was partly explained by our preliminary computational study.[20] A more comprehensive understanding of the triple action mechanism of *l*-SPD against D1R, D2R, and D3R at the atomic level is fundamental for developing superior antipsychotics. Obviously, the 3D structures of D1R and D2R are indispensable for computationally figuring out the triple action mechanism. Unfortunately, only the 3D structure of D3R is currently available.

It has been widely recognized that molecular modeling and simulation are an excellent complement to experiments in explaining experimental results and guiding further experiment design.[20,21] Furthermore, additional information that is not accessible by experiments can be revealed by computational approaches.[22] In the absence of experimental structures, computational homology modeling methods based on high sequence identity can be employed to predict the 3D models with enough accuracy, which can subsequently be used to aid in the understanding of protein functional mechanisms.[23] Molecular dynamics (MD) simulations, taking advantage of iteratively tracking the trajectory of conformational change, can provide information about the conformational properties of molecular system and the way in which the conformation changes with time, such as the binding process of a ligand into a protein's binding pocket, the binding conformation that the ligand and protein adopt, and other time-dependent properties.

With the recent insightful information about the activation mechanism of GPCR,[24,25] as well as the advent of the active-state structure of β_2AR[4,5] and the inactive-state structure of D3R,[11] we are motivated to perform a more comprehensive computational study on D1R, D2R, and D3R to explore the underlying agonistic and antagonistic mechanisms of *l*-SPD, which is essential for developing superior antipsychotics. Thus, homology modeling, automated molecular docking, and MD simulations are integrated in this study with the eventual aim to develop novel superior antipsychotic agents with less side effects and tailor these agents to possess the designed properties for individual therapy.

MATERIALS AND METHODS

Homology Modeling of D1R and D2R. The amino acid sequences of D1R and D2R were collected from the UniProtKB database (accession code: P21728 for D1R and P14416 for D2R), and sequence similarity searches for D1R and D2R were performed using the NCBI BLAST server.[26] The newly disclosed active-state structure of β_2AR (PDB code: 3P0G)[4] was selected as the template to construct the agonistic conformation of D1R, while for D2R homology modeling, the inactive-state structure of D3R (PDB code: 3PBL)[11] was used as the template as it shares a sequence identity of ∼78% with D2R in transmembrane (TM) regions. Sequence alignments of D1R and D2R with their templates were carried out using ClustalX 2.0.11 program.[27] The homology modeling and loop refinement were optimized with Modeler 9v4.[28] Fifty homology models were generated for both D1R and D2R after loop refinement, and the one with the lowest DOPE score[28] was adopted for subsequent energy minimization. The canonical disulfide bridge between residues C3.25 (in Ballesteros−Weinstein numbering, a single most conserved residue among the class A GPCRs is designated *x*.50, where *x* is the transmembrane helix number. All other residues on that helix are numbered relative to this conserved position) at the tip of TM3, and cysteine of ECL2 in the middle of extracellular loop 2 (ECL2) was created by using SYBYL 6.9.[29] The resultant models were subjected to 1000 cycles of steepest descent and 1000 cycles of conjugate gradient energy minimization. The PROCHECK[30] program which analyzes the residue-by-residue geometry and overall structure quality was employed to evaluate the stereochemical quality of the energy-minimized models of D1R and D2R. The starting structure of D3R in the simulation study comes from the crystal structure (PDB code: 3PBL).

Parameterization of *l*-SPD and Molecular Docking. The geometry of *l*-SPD was built based on its crystal structure[31] using the SYBYL 6.9 program and optimized at the DFT/B3LYP/6-31G** level. It features the same configuration and conformation as our previous study.[20] The partial atomic charges of *l*-SPD was determined with the DFT/B3LYP/6-31G** basis set by using the Gaussian 09 program.[32] Parameterization and topology generation of *l*-SPD for CHARMM force field were performed by using the Paratool plug-in of VMD.[33] The automated molecular docking program AutoDock4.0 with AutoDock Tools was employed to probe the possible complex of *l*-SPD bound with energy-minimized dopamine receptors (D1R, D2R, and D3R). Binding energy prediction was carried out using X-Score.[34] All available experimental data in combination with the lowest binding free energy were used to select the initial structure for subsequent MD simulations.

System Setup. The orientation of D1R, D2R, and D3R were adjusted using VMD, and their principal axis of symmetry was aligned to the *z*-axis using Orient plug-in of VMD. Helmut Grubmuller's SOLVATE program was then used to solvate the proteins followed by elimination of water molecules located in the hydrophobic protein−membrane interface. A pre-equilibrated rectangular patch of POPC membrane bilayer with solvated lipid headgroups was generated by using the Membrane Builder plug-in of VMD. The partially solvated proteins were immersed in the POPC membrane bilayer by matching the center of mass of proteins with that of membrane, respectively. The resulting placement of each receptor in

dx.doi.org/10.1021/jp3049235 | J. Phys. Chem. B 2012, 116, 8121−8130

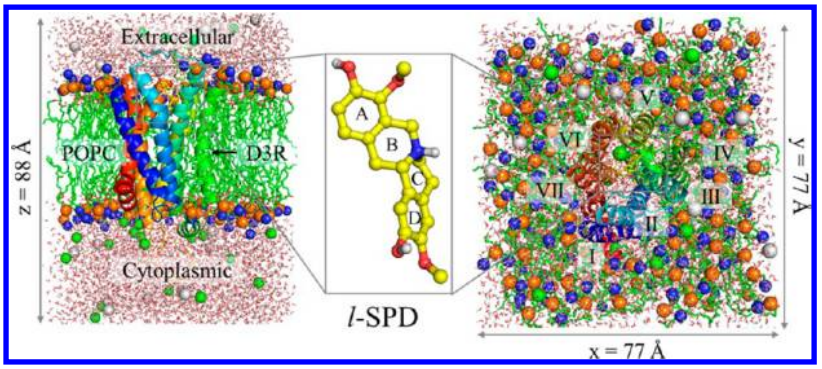

Figure 1. Side view (left) and top view (right) of *l*-SPD-D3R complex embedded in a hydrated POPC lipid bilayer. Protein is shown in cartoon representation, with *l*-SPD in ball and stick representation (middle). Water molecules are shown as lines, and lipid molecules are represented by sticks with their nitrogen (blue sphere) and phosphorus (orange sphere) atoms in van der Waals representation. Na^+ and Cl^- ions are also shown as gray and green spheres, respectively. All nonpolar hydrogen atoms are omitted for clarity.

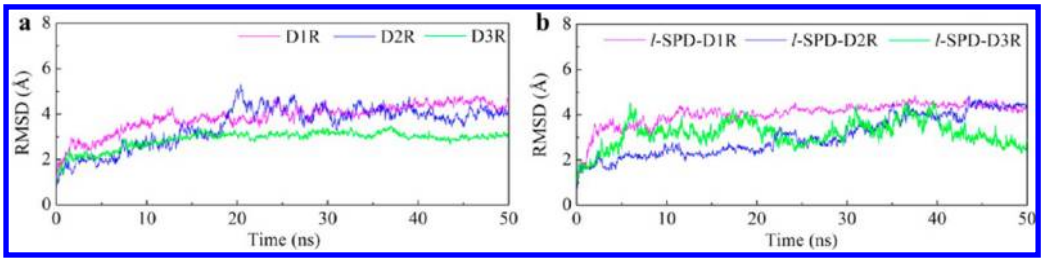

Figure 2. Root-mean-square deviation (rmsd) of the backbone atoms (CA, N, C) of all six simulation systems as a function of simulation time: (a) backbone rmsd for unliganded DRs; (b) backbone rmsd for *l*-SPD-DRs.

membrane was in agreement with the suggestions from the Orientations of Proteins in Membranes (OPM) database.[35] Lipids whose phosphorus atom lies within the region of the protein and those within 0.6 Å of the protein were removed. The protein−membrane complex was further solvated using the VMD Solvate plug-in. Water molecules added inside the lipid bilayer and the proteins were eliminated. The VMD Autoionize plug-in was then employed to create an ionic concentration of 150 mM NaCl by transmuting random water molecules into Na^+ and Cl^- and to neutralize the system. A brief summary of the configuration of each final system is listed in Table S1, and a snapshot of one of the constructed simulation system (*l*-SPD bound D3R system) is shown in Figure 1.

Molecular Dynamics Simulation Parameters. All MD simulations were carried out using the parallel molecular dynamics program NAMD 2.6[36] and the CHARMM27 force field[37] with CMAP terms[38] for all protein molecules, POPC lipid molecules, and ions along with the TIP3P model[39] for water molecules. A cutoff of 12 Å (switching function starting at 10 Å) for van der Waals interactions was imposed. The particle-mesh Ewald technique[40] was employed to calculate long-range electrostatic forces without cutoff. Periodic boundary conditions were imposed on all simulations with an integration time step of 2 fs to allow a multiple time stepping algorithms to be employed. The simulations were equilibrated as an NPT ensemble, using the Langevin Nosé−Hoover method[41] to maintain the pressure at 1 atm, and the temperature was kept at 310 K by using Langevin dynamics with a very weak friction coefficient.

Molecular Dynamics Simulation Protocol. All simulation systems were first subjected to 1000 cycles of steepest descent and 1000 cycles of conjugate gradient energy minimization followed by a 0.5 ns equilibration with protein, water, ions, and lipid headgroups held fixed to allow the melting of lipid tails. Subsequently, 1000 cycles of minimization followed by a 0.5 ns equilibration was effected with harmonic constraint on protein so as to guide the system to the nearest local energy minimum. During this stage, forces were applied to water molecules entering the highly hydrophobic membrane−protein interface to prevent this region from hydration. After minimization and equilibration with the protein constrained, the harmonic constraint was released to permit the whole system to equilibrate for 0.5 ns further. Production runs were finally conducted for 50 ns for all systems.

RESULTS AND DISCUSSION

3D Structures of D1R, D2R, and D3R. Sequence alignment indicated that the sequence identity in transmembrane helices was 42.4% between D1R and β_2AR and 72.9% between D2R and D3R, respectively (Figure S1). The 3D models of D1R and D2R were constructed using the newly resolved agonist-state crystal structure of β_2AR and antagonist-state X-ray structure of D3R as templates, respectively. The PROCHECK statistics calculations showed that 100% of the residues in our D1R and D2R models were either in the most favored or in the additionally allowed regions of the Ramachandran plot (Figure S2), suggesting that the overall main-chain and side-chain conformations are much more reliable as compared with our previous models. The previous models of D1R and D2R were built by taking bovine rhodopsin as the template, which was the only crystallized structure in GPCR family at that time and had ca. 25% sequence identity in TM region with D1R and D2R. The overall architecture of our present D1R and D2R models is similar to that of our previously reported DRs. Similar to previous D1R and D2R models, three intramolecular hydrophobic interaction clusters

dx.doi.org/10.1021/jp3049235 | J. Phys. Chem. B 2012, 116, 8121−8130

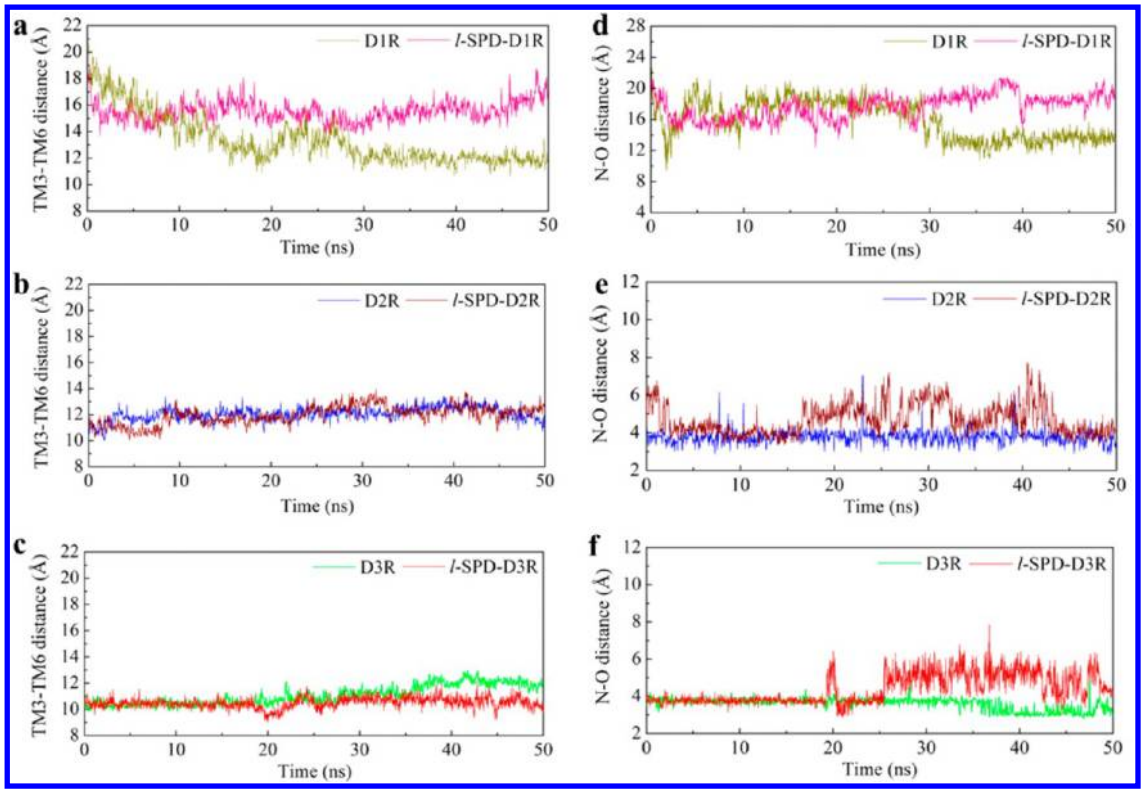

Figure 3. Distance fluctuations in TM3−TM6 and N−O during the MD simulations.

for both D1R and D2R were found: cluster 1 is surrounded by TM3, TM6, and TM7; cluster 2 is in TM2 and TM4; and cluster 3 is in TM3 and TM5.[20] However, differences are observed at the cytoplasmic face of D1R, with an outward movement of TM5 and TM6 and an inward movement of TM3 and TM7 in the present model. Such movement of transmembrane segments is a typical feature of activated β_2AR.[4] As the present D1R model was constructed based on the active-state β_2AR, it is presumably in an active state and is more suitable for investigating the agonist effect of *l*-SPD.

Cytoplasmic Helical Movement in Agonistic D1R and Antagonistic D2R/D3R. The three molecular systems assembled by embedding D1R, D2R, and D3R in a rectangular box comprising a POPC lipid bilayer surrounded by explicit water were simulated for 50 ns each. The MD simulations showed that, for all systems, temperature, mass density, and volume were relatively stable after 2 ns. After that, the fluctuation scale became much smaller for the rms deviations of the backbone atoms of all simulation systems (Figure 2), indicating that the molecular systems behaved well thereafter.

The most prominent differences in conformation between active and inactive GPCRs are resided at the cytoplasmic face, with the outward movement of TM3 and TM6, as exemplified by the active crystal structures of β_2AR-T4L-Nb80 and β_2AR-Gs complexes[4] and by the active crystal structures of opsin receptor.[42] A systematic examination of currently available GPCR crystal structures revealed that the movement of TM6 apart from TM3 is the key event in the process of GPCR activation (Table S2), as such conformational change opens the docking pocket for G protein. The distances between TM3 and TM6 in the cytoplasmic ends (distance between centroid of the Cα atoms of four residues located at the tip of each TM) were monitored for both liganded and unliganded D1R, D2R, and D3R as shown in Figure 3. The separation in TM3-TM6 for D1R shortened gradually from ca. 20 Å to ca. 12 Å at the first 30 ns and remained stable for the rest 20 ns in its unliganded state simulation. It indicated that a transition from active state to inactive state is through a continuum of intermediate conformations; this kind of behavior is in consistency with the postulate proposed by Brian Kobilka et al. that GPCRs are more like molecular rheostats that are able to sample a continuum of conformations.[25] Upon binding with *l*-SPD, the separation in TM3−TM6 was kept at ca. 15 Å (above 14 Å) during the entire simulation (Figure 3a), implying that *l*-SPD has the capacity of stabilizing D1R in its active state. In contrast to the conformational changes induced by *l*-SPD in D1R, *l*-SPD-induced conformational changes at the cytoplasmic faces of both D2R and D3R were not remarkable. The separation in TM3−TM6 in unliganded D2R is relatively stable and is kept at ca. 12 Å during the entire simulation. While in *l*-SPD bound D2R, the separation in TM3−TM6 fluctuated slightly at around 11 Å during the first 8 ns, and then it jumped to ca. 12 Å. As for D3R, the overall landscape of distance in TM3−TM6 is stabilized at 10−11 Å in both liganded and unliganded D3Rs (Figure 3b,c).

Ionic Lock Formation/Breakage in Agonistic D1R and Antagonistic D2R/D3R. It is also established that the basal conformation of GPCRs are maintained by interhelix loops and noncovalent interactions between side chains of a set of crucial residues in TM regions.[24] One of the best characterized examples of noncovalent interaction is a salt bridge formed between R3.50, part of the highly conserved (D/E) RY motif in transmembrane helix 3, and the conserved E6.30 in transmembrane helix 6. This salt bridge network was nicknamed "ionic lock".[43] Though it was originally proposed to account for the activation of β_2AR, accumulated studies have demonstrated that this interaction was crucial in stabilizing the inactive state of the rhodopsin family GPCRs.[43,44] In order to get a more

dx.doi.org/10.1021/jp3049235 | J. Phys. Chem. B 2012, 116, 8121−8130

detailed understanding of dopamine receptor behaviors before and after ligand binding, the separation between the centroid of atoms CZ, NH1, NH2 in R3.50 and that of atoms CD, OE1, OE2 in E6.30 termed "N−O distance" (Figure S3) was monitored and was chosen as an indicator of ionic lock formation.

The ionic lock formed between R3.50 in the E/DRY motif and E6.30 was proposed to have an essential role in maintaining GPCRs in an inactive state. In the simulation of unliganded D2R, the N−O distance between R3.50 and E6.30 was stably confined below 3.8 Å (Figure 3e); it indicated that R3.50 formed a stable ionic lock with E6.30 during MD simulation. However, in the case of the *l*-SPD-bound D2R, the corresponding N−O distance fluctuated between 3 and 7 Å, indicating that the ionic lock slightly fluctuated upon antagonist binding. Similar to the unliganded D2R system, N−O distance of unliganded D3R was well conserved at ca. 3.8 Å within the first 38 ns of the simulation, and then it decreased to 3 Å after 38 ns, which signified a reinforcement of the ionic lock. While for the *l*-SPD bound D3 receptor, the ionic lock ruptured at ca. 26 ns, the corresponding N−O distance even upsurged to 5 Å (Figure 3f). In terms of unliganded D2R and D3R, the important feature in unliganded D1R simulation is that no ionic lock is established (Figure 3d), but the distance in the TM3−TM6 at the intracellular ends decreased to ca. 12 Å. In contrast, the corresponding distance kept almost constant (16−20 Å) in the simulation of *l*-SPD-bound D1R, showing the important role of *l*-SPD in stabilizing the active state of D1R. It supports the point that the breakage of ionic lock is one of the features in the active D1R.

Functionally Relevant Interaction between *l*-SPD and D1R, D2R/D3R. The predicted binding energies of *l*-SPD for D1R, D2R, and D3R are very well correlated with the experimental values as shown in Table 1 and Figure 4.

Table 1. Predicted and Experimental Binding Energies of *l*-SPD with D1R, D2R, and D3R

receptor	predicted binding energy (kcal/mol)	experimental binding energy (kcal/mol)
D1R	−11.00	−10.80
D2R	−9.98	−9.60
D3R	−10.72	−10.66

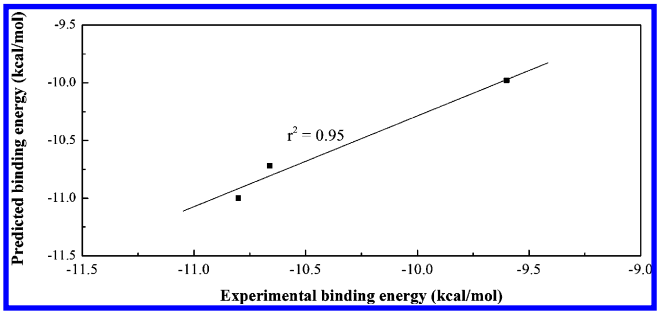

Figure 4. Correlation between predicted binding energy and experimental binding energy.

Although there are deviations between the experimental value (−10.80, −9.60, and −10.66 kcal/mol)[15] and predicted data, the general trend is that *l*-SPD binds to D1R and D3R more strongly than to D2R.

The differences in binding pocket lining among D1R, D2R, and D3R were initially compared aiming at elucidating the triple mechanism of *l*-SPD. Of the 18 interacting transmembrane residues with *l*-SPD, 9 were conserved in all complexes and all 18 residues in both D2R and D3R were strictly conserved as revealed by sequence alignment in binding pocket (Figure 5g). Their binding pocket shapes were different (Figure 5d−f). Specifically, in D2R and D3R, the large binding pocket 1 located between TM3, TM5, TM6, and TM7 was slightly narrower than the corresponding binding pocket 1 in D1R; such narrowness was presumably resulted from the relative bulkiness of the imidazole side chain H6.55 in D2R and D3R with respect to the amide side chain of N6.55 in D1R. Additionally, there was also a significant difference in the orientation between Y7.43 of D2R and D3R and W7.43 of D1 in which Y7.43 pointed toward extracellular side, while W7.43 was directed toward cytoplasmic side. As a result of such difference, the binding pocket 2 of both D2R and D3R were separated from pocket 1, whereas in D1R, binding pocket 2 was merged with pocket 1. Previous efforts to rationalize the structural basis of selectivity have also focused on binding regions that are not conserved among DR subfamily, with primary attention being given to ECL2.[11,45,46] In D1R, C186, D187, and S188 of ECL2 were found to be in contact with *l*-SPD with their counterparts in D2R and D3R being C182, I183, I184 and C181, S182, I183, respectively.

Functionally relevant interactions between *l*-SPD and D1R, D2R, and D3R were then investigated to understand the agonistic and antagonistic mechanism of *l*-SPD. Hydrogen bonding, electrostatic (red dashed lines), and hydrophobic interactions were observed as major contributions to *l*-SPD binding. As a common binding feature, *l*-SPD employed its protonated nitrogen atom to form electrostatic attraction with negatively charged D3.32 in D1R, D2R, and D3R (Figure 5a−c), such a common interaction was in well agreement with the fact that D3.32 plays an essential role in ligand binding to aminergic GPCRs.[45]

Despite the common binding features, differences in the binding interactions of *l*-SPD with all three receptors were remarkable. In the *l*-SPD−D1R complex, the binding orientation of *l*-SPD with D1R was reversed as compared to the binding orientations of *l*-SPD with D2R and D3R (Figure 5h). Given that the structure of *l*-SPD has one substructure of dopamine resided on both ends, this reversion of orientation was reasonable (Scheme 1). In addition, this adjustment of binding orientation of *l*-SPD with D1R was optimal for the formation of two hydrogen bonds (D ring hydroxyl group D−OH with side chain of N6.55 and A ring hydroxyl group A−OH with D175 of ECL2) (Figure 5a). These two hydrogen-bonding interactions were critical for the binding affinity of *l*-SPD with D1R as experimental results showed that simultaneous substitution of A−OH and D−OH by methoxyl groups resulted in a ca. 60-fold loss of binding affinity,[18] while monosubstitution of either A−OH or D−OH by a methoxyl group resulted in a ∼6-fold loss of binding affinity (Table S3, entries 1 and 4).[18] This binding mode is further supported by site-directed mutagenesis in β_2AR in which N6.55 was demonstrated to be involved in a hydrogen bonding to the *β*-OH group of adrenaline.[47−49] Furthermore, Manivet and co-workers showed that N6.55 in the 5-HT$_{2B}$ receptor is involved in direct or indirect 5-HT binding.[50]

In *l*-SPD-D2R and *l*-SPD-D3R complexes, the overall interaction landscape is similar to each other but with the orientation of *l*-SPD reversed relative to that in D1R as previously mentioned. In both *l*-SPD-D2R and *l*-SPD-D3R, the

dx.doi.org/10.1021/jp3049235 | J. Phys. Chem. B 2012, 116, 8121−8130

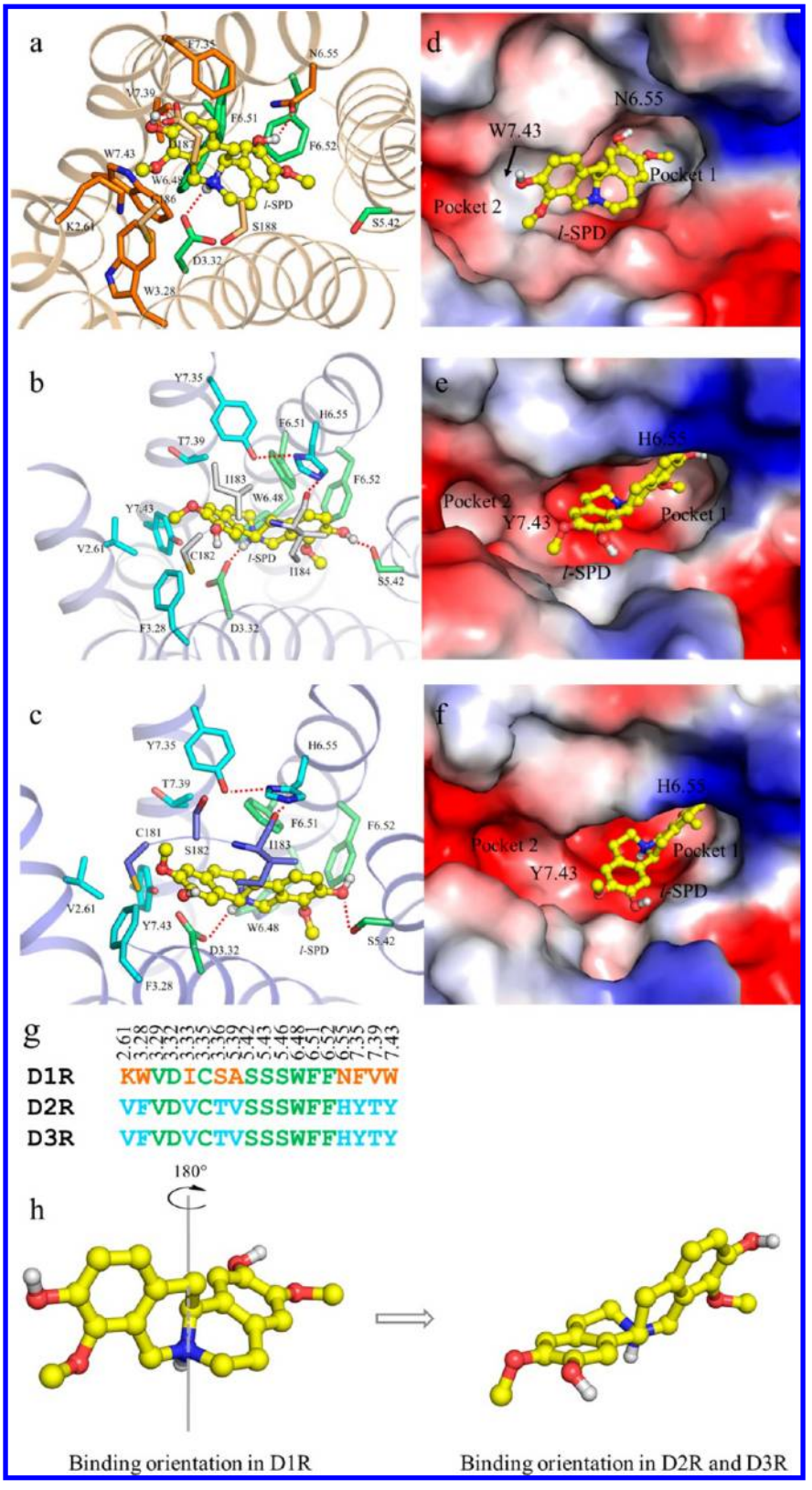

Figure 5. Binding pocket characteristics of D1R, D2R, and D3R. (a, b, and c) Binding pocket lining of D1R, D2R, and D3R. (d, e, and f) Binding pocket shape of D1R, D2R, and D3R. (g) Binding pocket residue sequence alignment of D1R, D2R, and D3R. (h) Binding orientations of *l*-SPD in D1R, D2R, and D3R. Residues colored in green are conserved in the binding of *l*-SPD with D1R, D2R, and D3R; those colored in cyan are conserved in the binding of *l*-SPD with D2R and D3R. Residues colored in orange are unique in the binding of *l*-SPD with D1R.

A-OH of *l*-SPD hydrogen bonded to S5.42 (Figure 5b,c), which is generally accepted as a key contributor to antagonist binding in both dopamine receptors and β_2AR.[49,51,52] This hydrogen bonding is important for *l*-SPD to bind with D2R since structural modification showed that the substitution of A-OH with a methoxyl group resulted in a ca. 12-fold loss of affinity

dx.doi.org/10.1021/jp3049235 | J. Phys. Chem. B 2012, 116, 8121−8130

Scheme 1. Simplification of *l*-SPD Structure

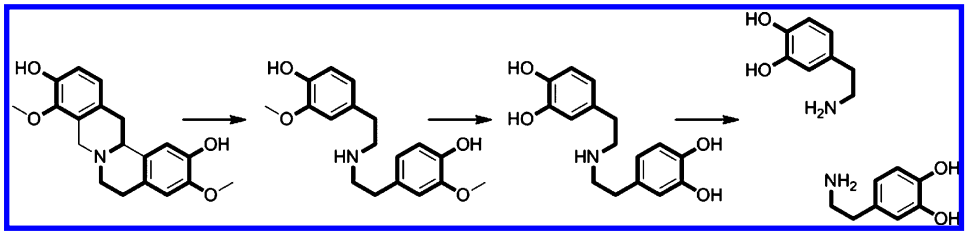

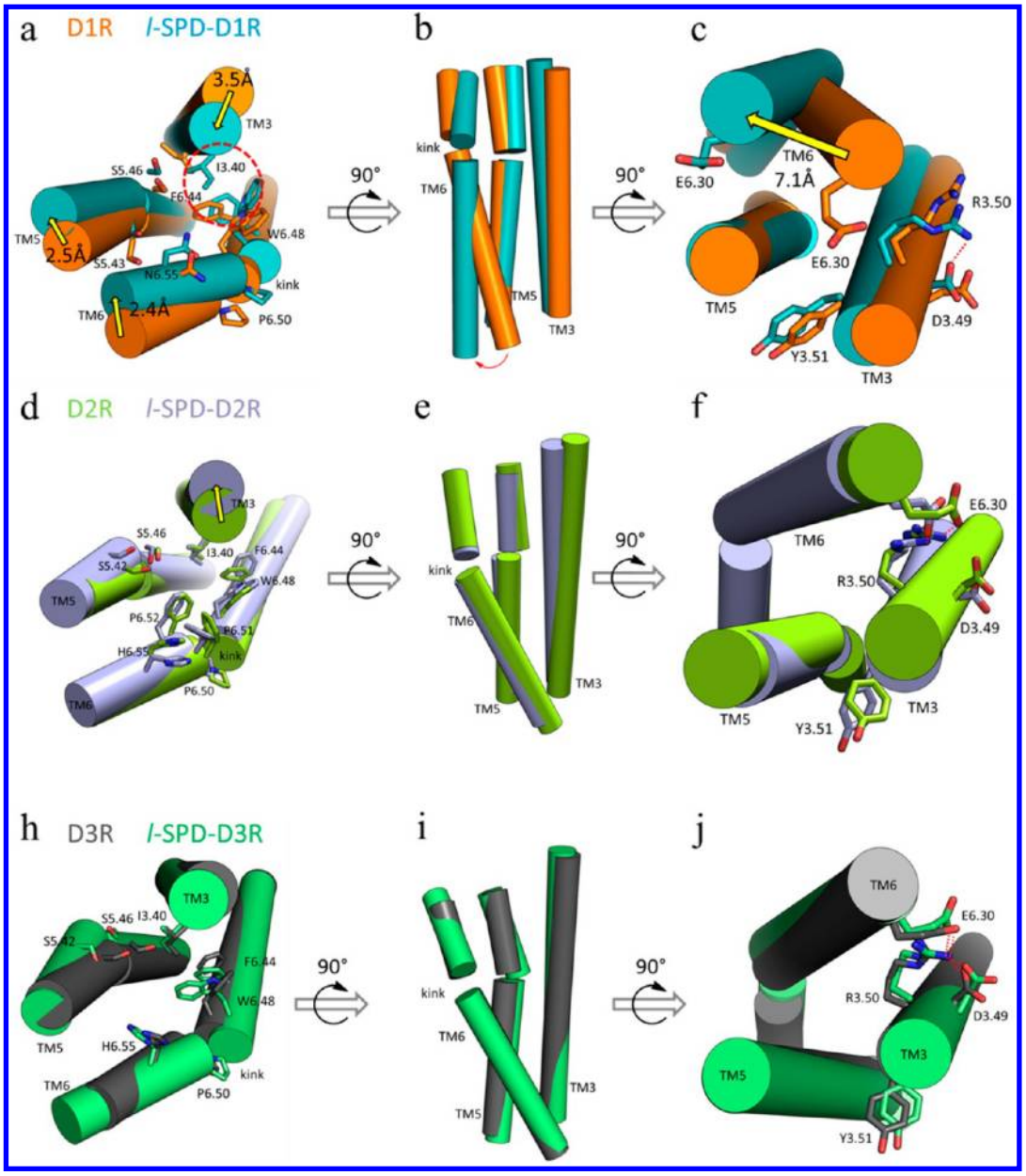

Figure 6. Mechanism for the triple action of *l*-SPD on D1R, D2R/D3R. (a, b, c) Agonistic mechanism of *l*-SPD on D1R. (d, e, f). Antagonistic mechanism of *l*-SPD on D2R. (h, i, j) Antagonistic mechanism of *l*-SPD on D3R.

(Table S3, entries 1 and 3).[18] However, no direct hydrogen bonding is established by ring D of *l*-SPD neither in D2R nor in D3R. Another key interaction in *l*-SPD-D2R and *l*-SPD-D3R complexes is that the A ring of *l*-SPD is involved in energetically favorable edge-to-face aromatic stacking with F6.51, F6.52, and H6.55 (Figure 5b,c), while in *l*-SPD-D1R, hydrophobic stacking is expensed for the formation of hydrogen bond (see above discussion).

It is also worthy to note that N6.55 of D1R was hydrogen bonded to D-OH of *l*-SPD through its side-chain amide carboxyl oxygen, whereas as the counterpart of N6.55, H6.55 in D2R and D3R served as a bridge between TM6 and ECL2, it contributes to the internal structural stability of the receptor by

dx.doi.org/10.1021/jp3049235 | J. Phys. Chem. B 2012, 116, 8121−8130

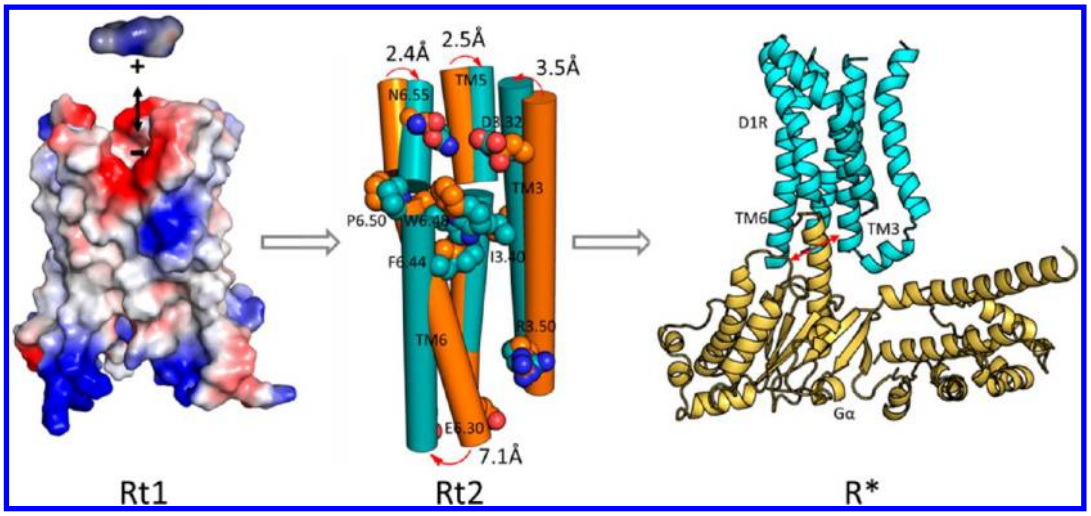

Figure 7. Proposed activation process of the D1R by an *l*-SPD like agonist. Rt1: electrostatically induced binding of an agonist. Rt2: agonist binding-induced structural changes (cyan, agonist-bound state; orange, unliganded state; key residues are represented as spheres; red arrows indicate relative movement of TMs). R*: the fully activated D1R in complex with Gα (this model was constructed according to the complex of β2AR with G-protein).[53,54]

hydrogen bonding with Y7.35 and carbonyl group in backbone of I184 and I183, respectively, through its two imidazole nitrogen atoms (Figure 5b,c). As the amide side chain of N6.55 is relatively small, the binding pocket 1 of D1R is sterically unhindered, making this binding pocket optimal for the binding of D ring of *l*-SPD. On the contrary, the relative narrowness of binding pocket 1 of D2R and D3R caused by the bulkiness of H6.55 made it only suitable for the binding of A ring of *l*-SPD. Furthermore, *l*-SPD formed polar contact with K2.61 by methoxyl group in A ring of D1R, whereas in D2R and D3R, V2.61 exempted the formation of such polar contact.

Mechanism for the Triple Action of *l*-SPD on D1R, D2R/D3R. It is now interesting to speculate how *l*-SPD exerts its triple action on D1R, D2R, and D3R and how the differences in binding mode are coupled with structural behavior in the cytoplasmic regions of TM3 and TM6. As can be seen from the binding pocket lining shown in Figure 5, when bound to D1R, *l*-SPD formed hydrogen bond with agonist-sensitive residue in TM6 (N6.55) to mediate its agonist activity, while bound to D2R and D3R, energetically favorable edge-to-face aromatic stacking was found between *l*-SPD and TM6, and instead of hydrogen bonding to *l*-SPD, H6.55 formed two hydrogen bonds with Y7.35 and I184 and I183 of ECL2. A plausible conformational link is shown in Figure 6. Inactive and active D1R structures were superimposed to monitor structural changes in ligand binding site. As shown in Figure 6a, the greatest differences between inactive and active structures in the binding site are a 3.5 Å movement of the extracellular part of TM3 toward the core of the receptor, a clockwise rotation of the extracellular segment of TM6 and a slight bulge of TM5 at S5.46 toward TM3. Apparently, the clockwise rotation of the extracellular segment of TM6 is the result of the hydrogen bonding between the D-OH of *l*-SPD and N6.55 (Figure 5a). Such clockwise rotation in turn repositions F6.44 and W6.48 of TM6 to form a hydrophobic stacking with I3.40 of TM3, causing inward movement of the extracellular part of TM3, similar to the hydrophobic stacking observed in the activation of β_2AR.[4] Accompanying these structural changes, the cytoplasmic segment of TM6 shifts significantly (7.1 Å) toward lipid, exempting the formation of an ionic lock between R3.50 and E6.30; this shift in turn opens the docking pocket for G protein and leads to the activation of D1R (Figure 6b,c).Without binding of *l*-SPD, R3.50 and E6.30 approach gradually to mimic an inactive-state D1R (Figure 6c).

To investigate the structural determinant of antagonist effects of *l*-SPD on D2R, an unliganded D2R structure was superimposed to a typical *l*-SPD stabilized structure. In contrast to the relative transmembrane movements in *l*-SPD-bound D1R, no significant rotation is found in transmembrane helices in *l*-SPD-bound D2R (Figure 6d,e), except that the extracellular segment of TM3 moves away from the binding pocket as compared to unliganded D2R. In *l*-SPD-bound D1R, N6.55 moves toward the ligand binding site to form two hydrogen bonds with *l*-SPD. Though in *l*-SPD-D2R aromatic stacking was found between *l*-SPD and F6.51, F6.52 and H6.55, examination of the downstream hydrophobic residues I3.40, W6.48, and F6.44 indicated that those residues were not induced to fit for hydrophobic stacking (Figure 6d). The absence of such a critical hydrophobic stacking exempted an outward movement of the cytoplasmic segment of TM6 (Figure 6e). In turn, as can be seen in Figure 6f, the ionic lock between R3.50 and E6.30 was maintained when D2R was bound with *l*-SPD.

In the *l*-SPD-bound D3R model, prominent helical movement as compared to unliganded D3R is absent except that a bulge located at S5.46 is tilted slightly outward from the binding pocket to accommodate *l*-SPD. Though similar aromatic stacking was found between *l*-SPD and F6.51, F6.52, and H6.55 in the *l*-SPD-D3R complex, the absence of hydrophobic stacking immediately downstream precluded an inward movement of the extracellular segment of TM6 (Figure 6h). As a result, a significant outward movement of the cytoplasmic segment of TM6 is prevented (Figure 6i,j), and the ionic lock between R3.50 and E6.30 is maintained (Figure 6j).

Proposed Activation Process of D1R. Based on our structural modeling, MD simulations, and the previously reported signal transduction model of D1R,[20] a stepwise activation process of D1R is proposed. Typically, the D1R adopts the inactive state through its intramolecular interaction and transits between several energy minima conformations by molecular thermodynamic motion. As the protonated *l*-SPD

dx.doi.org/10.1021/jp3049235 | J. Phys. Chem. B 2012, 116, 8121−8130

diffuses to the extracellular mouth of the binding cavity of D1R, the electrostatic attraction between the negatively charged region of the D1R and positively charged *l*-SPD assists in their initial association (Figure 7, Rt1). The approach of extracellular ends of TM3 and TM6 to each other is then bridged by hydrogen bonding of *l*-SPD with N6.55 and electrostatic attraction with D3.32. As a result, I3.40, F6.44, and W6.48 are repositioned to form hydrophobic stacking, leading to a 7.1 Å outward movement of the cytoplasmic segment of TM6 (Figure 7, Rt2). At this stage, the receptor reaches its Rt2 state ready for G-protein binding, while not fully activated as experimental observation showed that both agonist and G-protein binding are required to fully activate GPCRs.[4,5] Finally, the large separation between the cytoplasmic ends of TM3 and TM6 allows readily binding of G-protein, leading D1R to its fully activated R* state. This stepwise activation process of D1R is supported by the currently accepted postulate about the dynamics of GPCRs; that is, GPCRs are more like molecular rheostats rather than simple two-state switches and are consistent with the activation mechanism of β_2AR.[5,24,25]

CONCLUSION

We report herein a more comprehensive molecular modeling and molecular dynamics simulation study of the unliganded D1R, D2R, and D3R and *l*-SPD-D1R, *l*-SPD-D2R, and *l*-SPD-D3R complexes, all simulated in a lipid bilayer membrane. New homology models of both D1R and D2R were constructed using the more reliable active state β2AR and inactive state D3R as templates, respectively. Structural analyses of molecular dynamics simulations were carried out followed by calculation of binding energy.

We found that the separation in TM3−TM6 for unliganded D1R shortened gradually from ca. 20 to ca. 12 Å, whereas the distance in TM3−TM6 was kept at ca. 15 Å during the entire simulation of *l*-SPD−D1R complex, and this kind of separation in TM3 and TM6 is a typical feature of active state GPCRs, while the distance in TM3−TM6 in all D2R and D3R simulations remained relatively stable below 14 Å, which is a typical feature of inactive state GPCRs. Although there was no ionic lock formed when the unliganded D1R relaxed to its inactive state, the ionic lock R3.60 and E6.30 approaches gradually to each other. Our predicted binding energies of *l*-SPD bound with D1R, D2R, and D3R correlated perfectly with experimental binding affinity, signifying that our *in silico* simulations probably resembled the binding poses of *l*-SPD to D1R, D2R, and D3R. A more in-depth analysis of the interaction maps of *l*-SPD with D1R, D2R, and D3R revealed that hydrogen bonding with N6.55 coupled with hydrophobic stacking between I3.40, F6.44, and W6.48 was the key feature to mediate the agonist effect of *l*-SPD on D1R, whereas the absence of hydrophobic stacking between I3.40, F6.44, and W6.48 in D2R and D3R excludes receptor activation.

Based on the observations from our structural modeling and molecular dynamics simulation, the agonistic and antagonistic dual-action mechanisms of *l*-SPD were proposed. In the agonistic mechanism of *l*-SPD on D1R, structural changes in transmembrane helices are ignited by the formation of a hydrogen bond between the hydroxyl group of ring D of *l*-SPD and N6.55 of TM6 which causes a clockwise rotation of the extracellular segment of TM6. Such clockwise rotation in turn repositions F6.44 and W6.48 of TM6 to form a hydrophobic stacking I3.40 of TM3, causing inward movement of the extracellular part of TM3. Accompanying these structural changes, the cytoplasmic segment of TM6 shifts significantly out of the receptor core, and this shift in turn opens the docking pocket for G protein and leads to the activation of D1R. However, in the antagonistic mechanism of *l*-SPD on D2Rand D3R, no hydrophobic stacking is formed between I3.40, F6.44, and W6.48 in D2R and D3R to lead to an outward movement of the cytoplasmic segment of TM6.

Our finding of key residues of D1R, D2R, and D3R involved in *l*-SPD binding could guide future experimental work on these receptors and has significance in the mechanism-based design of functional drugs targeting dopamine receptors.

ASSOCIATED CONTENT

Supporting Information

Sequence alignments of D1R with β_2AR and of D2R with D3R, Ramachandran plots of all DR models, a brief summary of all simulation systems, TM3−TM6 distances and ionic lock formation and breakage in representative active and inactive GPCR crystal structures, binding affinity data for *l*-SPD analogues, and the definition of N−O distance as an indication of ionic lock formation and breakage. This material is available free of charge via the Internet at http://pubs.acs.org.

AUTHOR INFORMATION

Corresponding Author

*Fax +86-21-50807188, Ph +86-21-50806600, e-mail kqyu@mail.shcnc.ac.cn (K.Q.Y.); Fax +86-21-51980010, Ph +86-21-51980010, e-mail wfu@fudan.edu.cn (W.F.).

Author Contributions

§These authors contributed equally.

Notes

The authors declare no competing financial interest.

ACKNOWLEDGMENTS

This work was supported by the National Natural Science Foundation of China (No. 81172919) and grants from the National High Technology Research and Development Program of China (863 Program) (No. 2012AA021102) and the State Key Program of Basic Research of China grant (2009CB918502).

REFERENCES

(1) Overington, J. P.; Al-Lazikani, B.; Hopkins, A. L. How many drug targets are there? *Nat. Rev. Drug Discovery* **2006**, *5*, 993−6.

(2) Cherezov, V.; et al. High-resolution crystal structure of an engineered human beta2-adrenergic G protein-coupled receptor. *Science* **2007**, *318*, 1258−65.

(3) Rosenbaum, D. M.; et al. GPCR engineering yields high-resolution structural insights into beta2-adrenergic receptor function. *Science* **2007**, *318*, 1266−73.

(4) Rasmussen, S. G.; et al. Structure of a nanobody-stabilized active state of the beta(2) adrenoceptor. *Nature* **2011**, *469*, 175−80.

(5) Rosenbaum, D. M.; et al. Structure and function of an irreversible agonist-beta(2) adrenoceptor complex. *Nature* **2011**, *469*, 236−40.

(6) Warne, T.; et al. Structure of a beta1-adrenergic G-protein-coupled receptor. *Nature* **2008**, *454*, 486−91.

(7) Warne, T.; et al. The structural basis for agonist and partial agonist action on a beta(1)-adrenergic receptor. *Nature* **2011**, *469*, 241−4.

(8) Jaakola, V. P.; et al. The 2.6 angstrom crystal structure of a human A2A adenosine receptor bound to an antagonist. *Science* **2008**, *322*, 1211−7.

(9) Xu, F.; et al. Structure of an Agonist-Bound Human A2A Adenosine Receptor. *Science* **2011**.

(10) Wu, B.; et al. Structures of the CXCR4 chemokine GPCR with small-molecule and cyclic peptide antagonists. *Science* **2010**, *330*, 1066−71.
(11) Chien, E. Y.; et al. Structure of the human dopamine D3 receptor in complex with a D2/D3 selective antagonist. *Science* **2010**, *330*, 1091−5.
(12) Payne, S. L.; Johansson, A. M.; Strange, P. G. Mechanisms of ligand binding and efficacy at the human D2(short) dopamine receptor. *J. Neurochem.* **2002**, *82*, 1106−17.
(13) Jentsch, J. D.; Roth, R. H. The neuropsychopharmacology of phencyclidine: from NMDA receptor hypofunction to the dopamine hypothesis of schizophrenia. *Neuropsychopharmacology* **1999**, *20*, 201−25.
(14) Castner, S. A.; Williams, G. V.; Goldman-Rakic, P. S. Reversal of antipsychotic-induced working memory deficits by short-term dopamine D1 receptor stimulation. *Science* **2000**, *287*, 2020−2.
(15) Jin, G. Z.; Zhu, Z. T.; Fu, Y. (-)-Stepholidine: a potential novel antipsychotic drug with dual D1 receptor agonist and D2 receptor antagonist actions. *Trends Pharmacol. Sci.* **2002**, *23*, 4−7.
(16) Dong, Z. J.; Guo, X.; Chen, L. J.; Han, Y. F.; Jin, G. Z. Dual actions of (-)-stepholidine on the dopamine receptor-mediated adenylate cyclase activity in rat corpus striatum. *Life Sci.* **1997**, *61*, 465−72.
(17) Jin, G. Z.; Huang, K. X.; Sun, B. C. Dual actions of (-)-stepholidine on dopamine receptor subtypes after substantia nigra lesion. *Neurochem. Int.* **1992**, *20* (Suppl.), 175S−178S.
(18) Mo, J.; et al. Recent developments in studies of l-stepholidine and its analogs: chemistry, pharmacology and clinical implications. *Curr. Med. Chem.* **2007**, *14*, 2996−3002.
(19) Cai, N. [A controlled study on the treatment of tardive dyskinesia using 1-stepholidine]. *Zhonghua Shen Jing Jing Shen Ke Za Zhi* **1988**, *21* (281−3), 319.
(20) Fu, W.; et al. Dopamine D1 receptor agonist and D2 receptor antagonist effects of the natural product (-)-stepholidine: molecular modeling and dynamics simulations. *Biophys. J.* **2007**, *93*, 1431−41.
(21) Li, Y. Y.; Hou, T. J.; Goddard, W. A., III Computational modeling of structure-function of g protein-coupled receptors with applications for drug design. *Curr. Med. Chem.* **2010**, *17*, 1167−80.
(22) Fu, W.; et al. Brownian dynamics simulations of the recognition of the scorpion toxin maurotoxin with the voltage-gated potassium ion channels. *Biophys. J.* **2002**, *83*, 2370−85.
(23) Cavasotto, C. N.; Phatak, S. S. Homology modeling in drug discovery: current trends and applications. *Drug Discovery Today* **2009**, *14*, 676−83.
(24) Kobilka, B. K.; Deupi, X. Conformational complexity of G-protein-coupled receptors. *Trends Pharmacol. Sci.* **2007**, *28*, 397−406.
(25) Rosenbaum, D. M.; Rasmussen, S. G.; Kobilka, B. K. The structure and function of G-protein-coupled receptors. *Nature* **2009**, *459*, 356−63.
(26) Altschul, S. F.; et al. Gapped BLAST and PSI-BLAST: a new generation of protein database search programs. *Nucleic Acids Res.* **1997**, *25*, 3389−402.
(27) Thompson, J. D.; Gibson, T. J.; Plewniak, F.; Jeanmougin, F.; Higgins, D. G. The CLUSTAL_X windows interface: flexible strategies for multiple sequence alignment aided by quality analysis tools. *Nucleic Acids Res.* **1997**, *25*, 4876−82.
(28) Sali, A.; Blundell, T. L. Comparative protein modelling by satisfaction of spatial restraints. *J. Mol. Biol.* **1993**, *234*, 779−815.
(29) Tripos International, SYBYL 6.9, 1699 South Hanley Rd., St. Louis, MO 63144.
(30) Laskowski, R. A.; Rullmannn, J. A.; MacArthur, M. W.; Kaptein, R.; Thornton, J. M. AQUA and PROCHECK-NMR: programs for checking the quality of protein structures solved by NMR. *J. Biomol. NMR* **1996**, *8*, 477−86.
(31) Xuan, J. C.; Lin, G. D.; Jin, G. Z.; Chen, Y. [Relevance of stereo and quantum chemistry of four tetrahydroprotoberberines to their effects on dopamine receptors]. *Zhongguo Yao Li Xue Bao* **1988**, *9*, 197−205.
(32) Frisch, M. J.; Trucks, G. W. ; Schlegel, H. B.; Scuseria, G. E.; et al. Gaussian, Inc., Wallingford, CT, 2010.
(33) Humphrey, W.; Dalke, A.; Schulten, K. VMD: visual molecular dynamics. *J. Mol. Graphics* **1996**, *14* (33−8), 27−8.
(34) Wang, R.; Lai, L.; Wang, S. Further development and validation of empirical scoring functions for structure-based binding affinity prediction. *J. Comput.-Aided Mol. Des.* **2002**, *16*, 11−26.
(35) Lomize, M. A.; Lomize, A. L.; Pogozheva, I. D.; Mosberg, H. I. OPM: orientations of proteins in membranes database. *Bioinformatics* **2006**, *22*, 623−5.
(36) Phillips, J. C.; et al. Scalable molecular dynamics with NAMD. *J. Comput. Chem.* **2005**, *26*, 1781−802.
(37) MacKerell, A. D., Jr.; et al. All-Atom Empirical Potential for Molecular Modeling and Dynamics Studies of Proteins. *J. Phys. Chem. B* **1998**, *102*, 3586−3616.
(38) Mackerell, A. D., Jr.; Feig, M.; Brooks, C. L., III Extending the treatment of backbone energetics in protein force fields: limitations of gas-phase quantum mechanics in reproducing protein conformational distributions in molecular dynamics simulations. *J. Comput. Chem.* **2004**, *25*, 1400−15.
(39) Jorgensen, W. L.; Chandrasekhar, J.; Madura, J. D. Comparison of simple potential functions for simulating liquid water. *J. Chem. Phys.* **1983**, *79*, 926−935.
(40) Darden, T.; York, D.; Pedersen, L. Particle mesh Ewald: An Nlog(N) method for Ewald sums in large systems. *J. Chem. Phys.* **1993**, *98*, 10089−10092.
(41) Martyna, G. J.; Tobias, D. J.; Klein, M. L. Constant pressure molecular dynamics algorithms. *J. Chem. Phys.* **1994**, *101*, 4177−4189.
(42) Scheerer, P.; et al. Crystal structure of opsin in its G-protein-interacting conformation. *Nature* **2008**, *455*, 497−502.
(43) Ballesteros, J. A.; et al. Activation of the beta 2-adrenergic receptor involves disruption of an ionic lock between the cytoplasmic ends of transmembrane segments 3 and 6. *J. Biol. Chem.* **2001**, *276*, 29171−7.
(44) Vogel, R.; et al. Functional role of the "ionic lock"--an interhelical hydrogen-bond network in family A heptahelical receptors. *J. Mol. Biol.* **2008**, *380*, 648−55.
(45) Shi, L.; Javitch, J. A. The binding site of aminergic G protein-coupled receptors: the transmembrane segments and second extracellular loop. *Annu. Rev. Pharmacol. Toxicol.* **2002**, *42*, 437−67.
(46) Shi, L.; Javitch, J. A. The second extracellular loop of the dopamine D2 receptor lines the binding-site crevice. *Proc. Natl. Acad. Sci. U. S. A.* **2004**, *101*, 440−5.
(47) Strader, C. D.; et al. Identification of residues required for ligand binding to the beta-adrenergic receptor. *Proc. Natl. Acad. Sci. U. S. A.* **1987**, *84*, 4384−8.
(48) Liapakis, G.; et al. The forgotten serine. A critical role for Ser-2035.42 in ligand binding to and activation of the beta 2-adrenergic receptor. *J. Biol. Chem.* **2000**, *275*, 37779−88.
(49) Wieland, K.; Zuurmond, H. M.; Krasel, C.; Ijzerman, A. P.; Lohse, M. J. Involvement of Asn-293 in stereospecific agonist recognition and in activation of the beta 2-adrenergic receptor. *Proc. Natl. Acad. Sci. U. S. A.* **1996**, *93*, 9276−81.
(50) Manivet, P.; et al. The serotonin binding site of human and murine 5-HT2B receptors: molecular modeling and site-directed mutagenesis. *J. Biol. Chem.* **2002**, *277*, 17170−8.
(51) Tomic, M.; Seeman, P.; George, S. R.; O'Dowd, B. F. Dopamine D1 receptor mutagenesis: role of amino acids in agonist and antagonist binding. *Biochem. Biophys. Res. Commun.* **1993**, *191*, 1020−7.
(52) Cox, B. A.; Henningsen, R. A.; Spanoyannis, A.; Neve, R. L.; Neve, K. A. Contributions of conserved serine residues to the interactions of ligands with dopamine D2 receptors. *J. Neurochem.* **1992**, *59*, 627−35.
(53) Rasmussen, S. G.; et al. Crystal structure of the beta2 adrenergic receptor-Gs protein complex. *Nature* **2011**, *477*, 549−55.
(54) Chung, K. Y.; et al. Conformational changes in the G protein Gs induced by the beta2 adrenergic receptor. *Nature* **2011**, *477*, 611−5.